

Rutherford Scattering

Kirsten A. Juhl ^{*1}, Henriette Ravn ^{†1}, and Laurits N. Stokholm ^{‡1}

¹*Department of Physics and Astronomy, Aarhus University*

September 23, 2018

Abstract

These experiments studies the Rutherford scattering of protons on atomic nuclei. Energetic 400 keV protons were generated using a Van de Graaff accelerator and directed onto thin metal foils of Au/C, LiF, B, and Al and the scattering cross section of the target atoms was measured as a function of the scattering angle in the range xx to 160 degrees. The cross section showed a clear angular dependency as as expected. The thickness of the target layers Au/C were determined from the stopping power of the layers to be The nuclear reactions of protons with boron were demonstrated by ... Mere is den dur bla bla bla ... In conclusion ...

elastic collisions in the semi-classical regime, governed by the Sommerfeld criterion for classical scattering. Paetz gen Schleck, *Nuclear Reactions: An introduction*, p. 14

This is usually fine for low energy physics, in which internal energies remain constant and no further particles are created or annihilated. For this experiment, which uses a single Van-de-Graaff accelerator to generate particles with energies of up to 400 keV, this is a good approximation.

1 Introduction

Almost all of our knowledge in the field of nuclear and atomic physics has been discovered through scattering experiments, and the theory of scattering underpins one of the most ubiquitous tools in physics. In low energy physics, scattering phenomena provide the standard tool to explore solid state systems. Historically, this was used as a first step towards our current understanding of the atom.

This paper examines the Rutherford scattering of a beam of 350 keV protons on a thin foil of a two layer Au/C target. To limit the extend of the paper, and to keep our discussion simple and relevant, we will only examine

2 Materials and Methods

Experimental Setup

To obtain energies up to 400 keV, a single Van-de-Graaff accelerator (see fig. 1) was used. The variety of incomming beam particles was limited by the source (a flask of hydrogen gas connected to the accelerator tank), which

^{*}201606487@post.au.dk

[†]20116112@post.au.dk

[‡]201605496@post.au.dk



Figure 1: The Van-de-Graaf accelerator.

was stationary and not changed. Therefore, we only consider incoming ions H^+ and H_2^+ . Acceleration of the ions was controllable by changing the voltage drop on the dashboard (see fig. 2) and thus also adjusting the kinetic energy of the incoming beam. This will be described further later on (see section Procedure).

The beamline was placed in an angle relative to the accelerator (see fig. 3). By changing the magnetic field strength of the electromagnet, one could choose which of the two possible incoming ions were deflected into the beamline and thus directed towards scattering on the target material at the end of the beamline. The motion of a charged particle in a magnetic field is governed by the Lorentz force law, and as the trajectory of the motion is traced as part of a circle, one obtains the necessary equality for the motion to be¹

$$F_m = QvB = F_{cp} = \frac{mv^2}{r}. \quad (1)$$

From this a ratio between the two magnetic

¹Concepts as forces and spatial confinements to circular paths is meaningful in the classical regime. This is not the case for a fully relativistic and quantum mechanical description.



Figure 2: Overview of dashboard. Closer graphics are seen in the Procedure.

fields needed for the respective ions is

$$R_B = \frac{B(H_2^+)}{B(H^+)} = \frac{m(H_2^+)v(H_2^+)}{m(H^+)v(H^+)} \quad (2)$$

$$2\frac{v(H_2^+)}{v(H^+)} = \sqrt{2}, \quad (3)$$

where it has been assumed that the mass of the two ions are related by $m(H_2^+) = 2m(H^+)$ and the speed of each ion is given as $v(X) = \sqrt{\frac{2E}{m(X)}}$. Given one of the magnetic fields, the other is determined from this ratio factor. The following magnetic field strengths were used:

$$B(H^+) = 1070 \text{ G} \quad B(H_2^+) = 1513 \text{ G} \quad (4)$$

Conclusively, by changing the magnetic field strength, one changes the incoming ion. However, the magnetic field strength can change over time scales of a measurement. This is a consequence of heating. The iron core is heated mechanically and thus its magnetic permeability changes. Also, the wire is heated electrically. As the resistance increases with temperature the current at a given potential will decrease; giving a lower effective magnetic field.

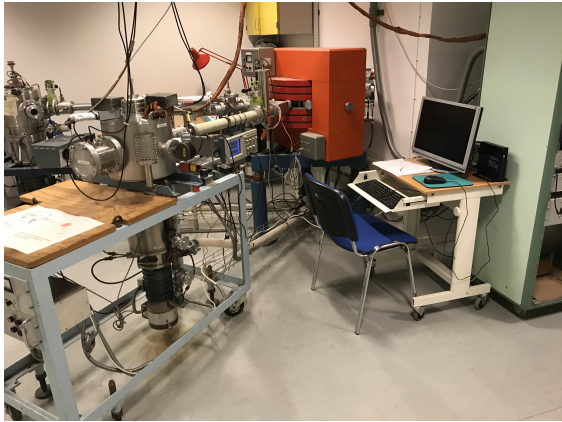


Figure 3: From left to right; Overview of the Faraday cup, Silicium detector, beamline, and electromagnet (red brick).

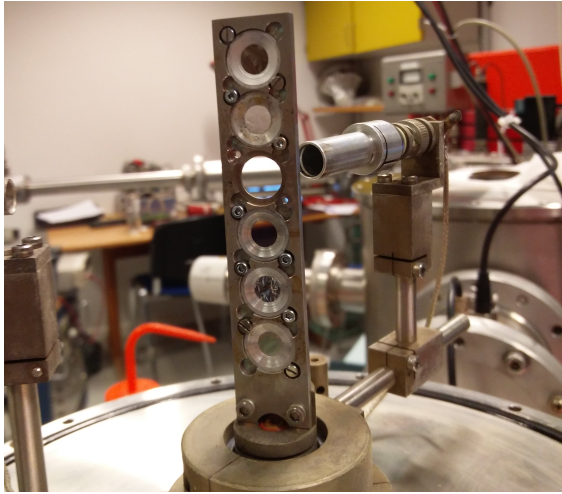


Figure 4: The equipment had a failure, so the targets were changed. We were lucky to get this picture of both detector and targets.

Subsequently, the incoming ions were directed towards the thin target foil (see fig. 4), and the scattered particles were detected by a Silicon detector at a variable angle up to 160 relative to the direct beam.

The detector was at a constant separation from the target, $r = 49 \pm 1$ mm, and it had a circular area of given diameter $D = 1,88 \pm 0,01$ mm. Of importance is the

solid angle of

$$d\Omega = \frac{dA}{r^2} \quad (5)$$

used in the Rutherford differential cross section later on.

The detector was coupled to a digitizer connected to a computer. During measurements the digitizer started a clock. When an ion was detected, the digitizer translated the measured energy into a digital number and sent the number and the corresponding time stamp to the computer. The program Mc2Analyzer was used to handle the data. The digital number is an arbitrary number called a channel number. It is translatable to the actual energy by a linear factor plus an offset. In order to convert these channel numbers to correct energies of the scattered particles a calibration was done.

Calibration

An energy measurement of the scattered ion gives a digital output, which we call a channel number (or bin number). These hold no physical interpretation, but can be translated to the equivalent energy of the scattered particle. To convert these channel numbers, a calibration is necessary.

Assuming a linear relationship between the energy and the channel number the energy can be found as

$$E = \alpha(k - k_0), \quad (6)$$

where k is the measured channel, k_0 is the channel number corresponding to a zero-amplitude input, and α is a conversion parameter. The parameters in the relation (see tab. 1) is determined by a two step program.

Determining the zero-amplitude constant

First, by connecting a pulser (variable output voltage), a relation between the varied energy and the corresponding channel number is obtained. We did this for equidistant pulsed energies, and although unimportant for the time being, we included the threshold pulser amplitude – the minimal amplitude for a detected signal.

Data obtained can be plotted as count numbers versus bin numbers. Due to the central limit theorem (Barlow, *Statistics, A guide to the use of statistical methods in the physical sciences*, p. 49), data can be fitted to a gaussian distribution. This is done for each value of pulsed energy, for which one gains parameter values for each gaussian within an uncertainty, determined by the square root of the covariance matrix diagonal (see fig. 5).

Each centroid (the mean bin number of the gaussian fit) was then compared as a function of the pulser amplitude. As expected from eq. (6), this follows a linear relation (see fig. 6). The intersection is interpreted as the bin number at zero amplitude (k_0).

Determining alpha

As described in the previous section, the magnetic field strength of the electromagnet can be adjusted to deflect either H^+ or H_2^+ into the beamline. For each of these a data point of energy related to channel number can be found at a given angle.

Table 1: The values of the parameters, used to convert channel numbers to energies.

Calibration parameters	
k_0	1.36 ± 0.15
α	0.800 ± 0.005

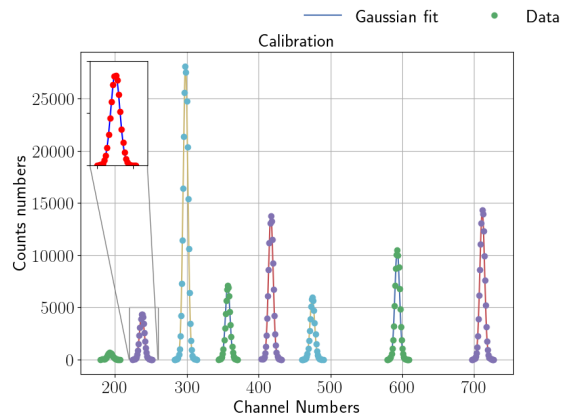


Figure 5: Gaussian fits for all data measured pulser-amplitude-signals. This was used to estimate the mean bin number (centroid), and the uncertainty of the parameters used in the energy-calibration.

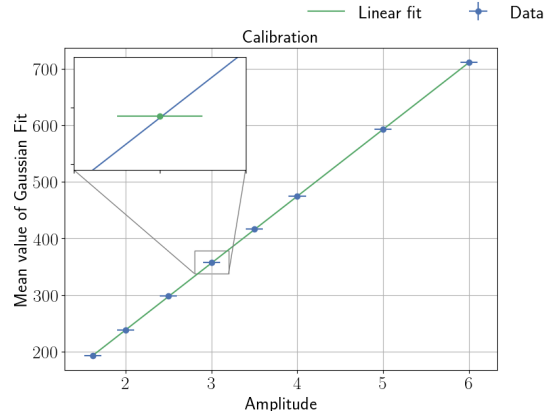


Figure 6: Linear fit of the mean values as a function of amplitude. This was used to determine the zero-amplitude constant k_0 .

The energy of the scattered particles, E_f , can be found by energy and momentum conservation considerations for elastic scattering in two dimensions. One is lead to the relation;

$$E_f = \left(\frac{m_p \cos \theta + \sqrt{m_t^2 - m_p^2 \sin^2 \theta}}{m_p + m_t} \right)^2 E_i, \quad (7)$$

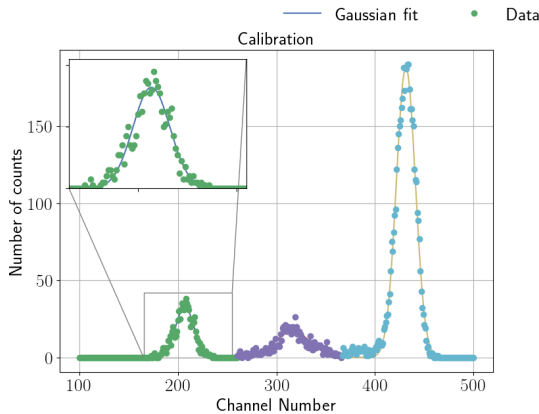


Figure 7: From left to right we see H_2^+ scattering off the gold layer and H^+ scattering off the carbon and gold layer respectively.

where E_i is the energy of the incident beam particles, m_p and m_t are the masses of the incident and the target particles, respectively. θ is the angle between the direct outgoing non-scattered beam and the scattered particles - also called the scattering angle.

Unfortunately, this only gives two data points one from H^+ and another from H_2^+ . Nonetheless, the incline from the linear fit to these data points is still useful. However, a work around solution for this specific problem exists. By using a target of two layers; gold and carbon respectively, we have multiple centroids; one for H_2^+ and the gold layer, another two for H^+ scattering off both gold and carbon (see fig. 7). Thus the linear fit (see fig. 8) has a third point.

One should be aware of the difference between the two linear fits. First we fitted for two parameters, both incline and intersection, and obtained the value of the zero-amplitude bin value (see fig. 6). Afterwards, we fitted for a single parameter, the incline, and used the value of k_0 (see fig. 8).

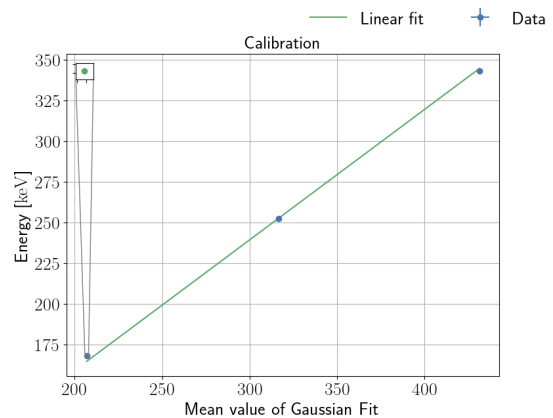


Figure 8: A linear fit of three points.

Targets

FIX The targets of interest in this experiment was a thin gold coated carbon plate. The gold coating was about one tenth of the carbon thickness. The thickness of the carbon plate have previously been determined as 250 Å, and the thickness of the gold coating as 25 Å.² The target was placed in holder, which contains several other targets. The height of the holder was fixed, though it was not investigated whether the marked height was optimal with respect to the beam position.

When measuring proton scattering at different angles, the blind angles of the target holder may cause a problem. In order to avoid the targets "blind-spots", the target was turned at an angle following the detector while still avoiding the incoming proton beam to hit a blind angle. The blind angles of the holder are around $\pm 30^\circ$ in each side of the target holder, see figure .

²The estimated thickness of each target available have been determined by the previous users of the experimental setup and written down on the whiteboard next to the setup.

Procedure

For a complete description of the experimental setup, we have provided this short review of the startup procedure. This can be omitted, but found valuable for the course examination.

First thing, the Van-de-Graaff. To accelerate the beam of incoming particles, one has to generate a high potential. Turning on the belt, one hears the mechanical rhumming. This will generate a potential difference as described further in Krane, *Introduction to Nuclear Physics*, p. 565.



Figure 9: The belt is turned on.

Now adjust the terminal voltage patiently towards the desired energy. Our lab instructor advised us to wait for each step, before going to the next.



Figure 10: Terminal voltage is adjusted to 350 keV.

Turn on the electromagnet. One can dial in the calculated magnetic field strength. This will do absolutely nothing to the experimental setup, but to translate the origin of the scale. To change the magnetic field strength, one has to change the current through the electromagnet.

Now open the vacuum valve, so the incoming ions can be detected. If the Faraday cup (detector for 0 degree scattering) is connected



Figure 11: Dashboard for the electromagnet.

to an Ampere meter, one can look for received current of charged particles. This should be maximized, by a variational principle about the calculated magnetic field, using the fine grid for adjustments.



Figure 12: Ampere meter connected to the Faraday cup to detect current of charged particles detected.

When the signal is good, there is one last step which is to set the output of the faraday cup from the Ampere meter to the input of the collector. This will give a precise count for the detected ions picked up in the faraday cup.



Figure 13: Collector with a timer. This can be set to stop counting after a time interval.

3 Angular dependency of the Rutherford cross section

The Rutherford differential cross section (Paetz gen Schleck, *Nuclear Reactions: An introduction*, p. 16) is given by

$$\left(\frac{d\sigma}{d\Omega}\right)_{\text{Rutherford}} = \left(\frac{Z_1 Z_2 e^2}{4E_\infty}\right)^2 \frac{1}{\sin^4(\frac{\theta}{2})} \quad (8)$$

where Z is the proton number of each interacting particle, E_∞ is the asymptotic energy, and θ is the scattering angle. If the energy is in MeV, this differential cross section will be in $\frac{\text{mb}}{\text{sr}}$.

This formula neglects the recoil energy of the target, which will be discussed later on.

Measurements

To test the angular dependency of the Rutherford cross section, we set the Silicium detector at a variable angle.

As mentioned earlier, the target has two layers, and thus the incomming beam of ions can scatter on both gold and carbon. As the Rutherford scattering is a coulomb interaction, we expect the gold layer to scatter the most at higher angles.

This is due to the change of the momentum of the incomming ion. Similar to a solar system.

To change the direction of the incomming ion, a big potential has to be generated by the target, much similar to the motion os comets closing in on the sun to leave it again. If not big enough the projectile will not change direction. As it is a coulomb interaction, the

However small, as the target has two layers, we will expect a double scattering. However

We meassured count numbers of the collector. The collector counted 10^{11} counts per

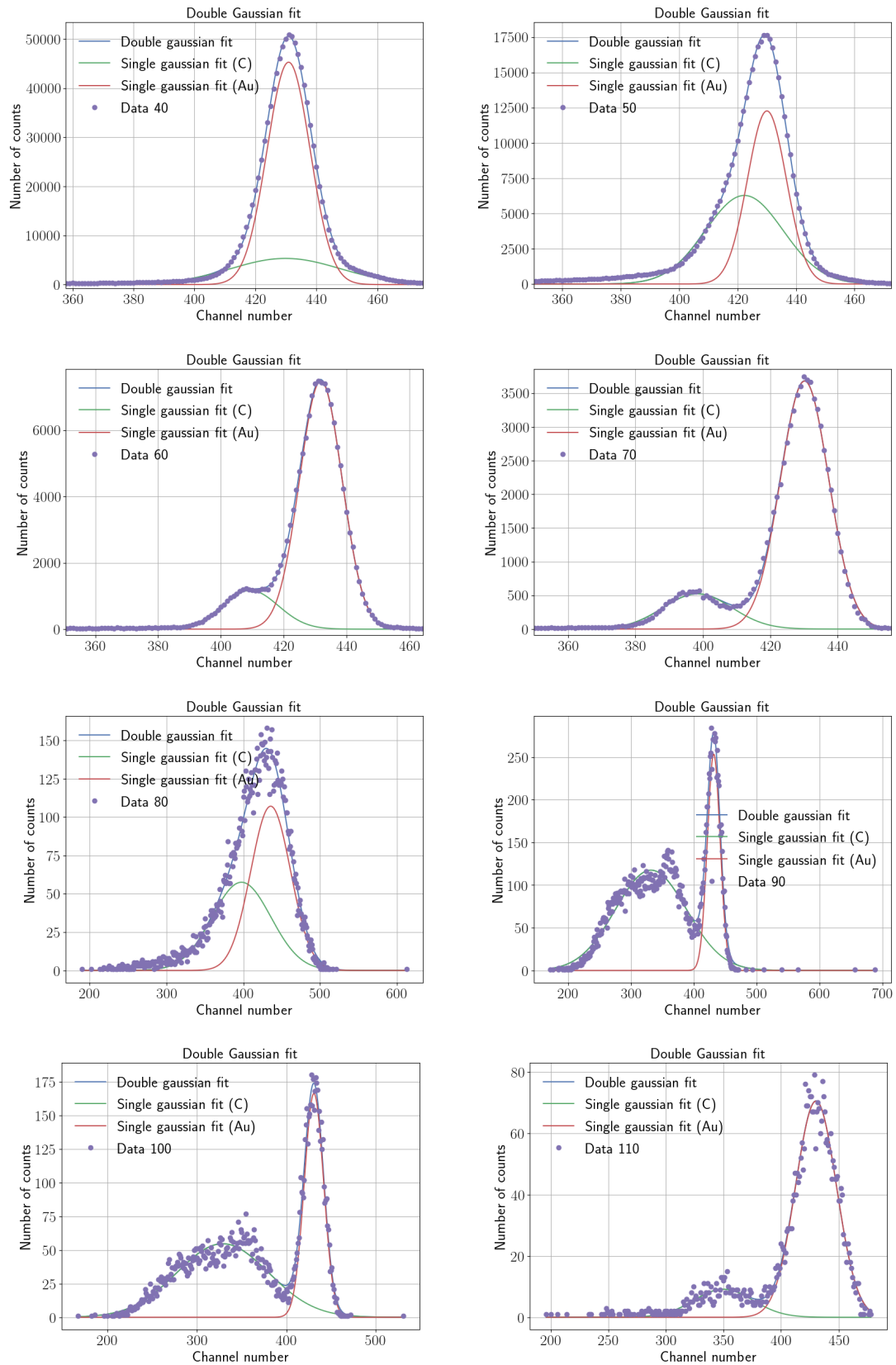
coulomb, and as there are $6,24150913 \cdot 10^{18}$ elementary charges per coulomb, we can related the count number to an amount of detected protons.

Now looking at data, one sees it is not a simple gaussian distribution. This is a conseuense of a double layered target, such the incomming hydrogen ion will scatter of both Carbon and Gold. Fitting a double gaussian, one gather six parameters. Amplitude, centroid and standard deviation of both gaussians. Here we use the linear combination of the two scattering processes.

Notice that the gaussian of greatest amplitude is corresponding to gold, which is in agreement with the relative sizes of the two atoms. Stable isotopes of gold has a nuclear number of $A_{\text{Au}} = 197$ whereas carbon has $A_{\text{C}} = 12$.

What is interestinglt is how the two peaks change relative position as a function of scattering, merging their gaussian distribution at low angles, and seperating at higher angles.

Using the calibration to convert the centroid channel number of each gaussian, we can plot the energies as a function of scattering angle.



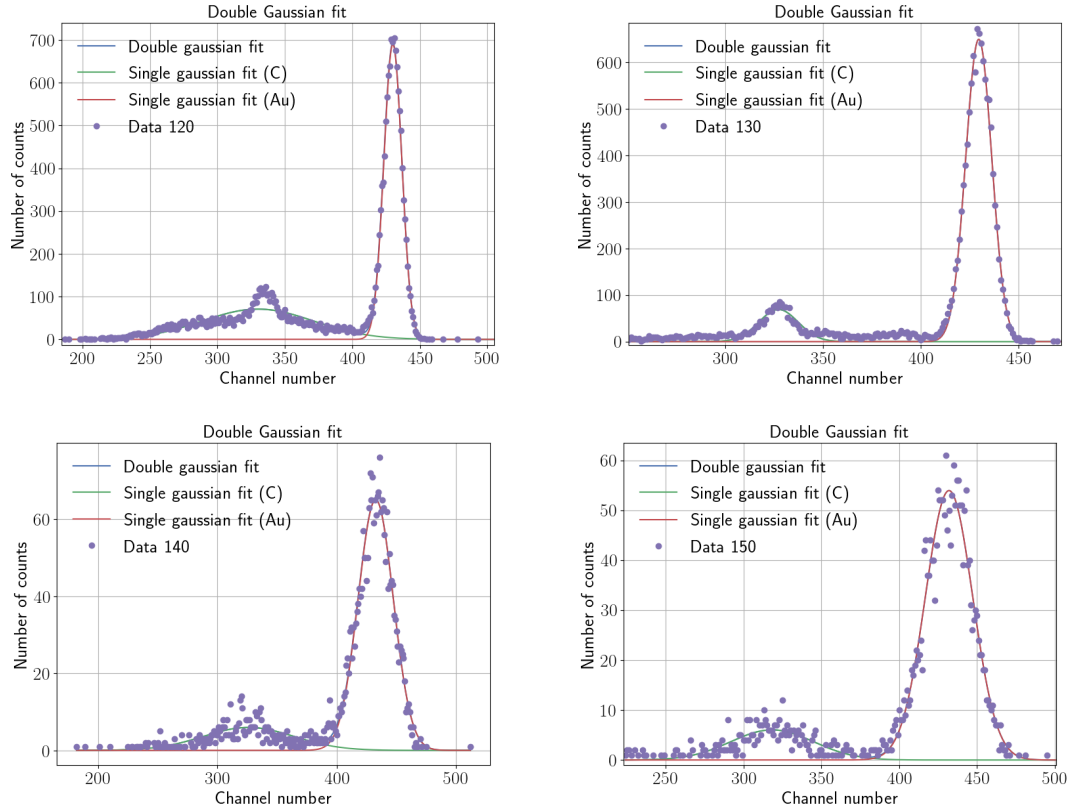


Figure 14: Angular dependency

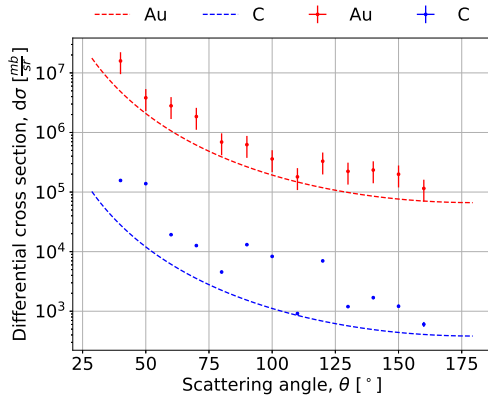


Figure 15: bb

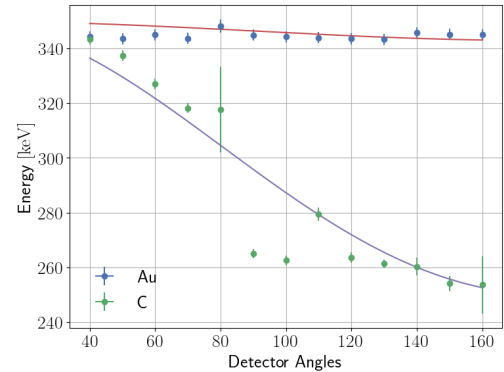


Figure 16: Energies of Carbon and Gold scattered compared to theoretical function.

4 Angular dependency of the proton energy

5 Target dependency of the Rutherford cross section

6 Thickness of the target layers

Most of the particles pass directly through the target without scattering however a small

amount gets scattered. When particles pass through the first layer the particles loose part of their energy, which means that the particles scattered on the second layer have lower energies when entering the second layer than if they had not passed through the first layer. By comparing measurements of scattering on the target with gold layer facing the beam and the carbon layer facing the beam, the distributions for scattering on carbon and gold are observed at different energies.

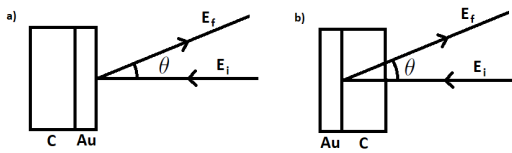


Figure 17: Sketch of how to determine thickness of the target carbon layer from the energy difference between: a) gold layer facing the beam and b) carbon layer facing the beam.

The changes in energies are proportional to the thickness of target layers. For the determination of the thickness of the carbon layer consider what happens to the energy in the two following situations. In situation a) gold is facing the beam, and the final energy is given as the incoming minus the energy lost due to scattering on gold:

$$E_{af} = E_i(1 - f_{Au}(\theta)),$$

where $f_{Au}(\theta)$ is the function giving the relation between the incoming energy E_i and the particle energy E_f in equation ?? after scattering on gold. In situation b) carbon is facing the beam, and the final energy is given as the incoming energy minus the energy lost due to the following: passing through the carbon layer, scattering on gold, and passing through

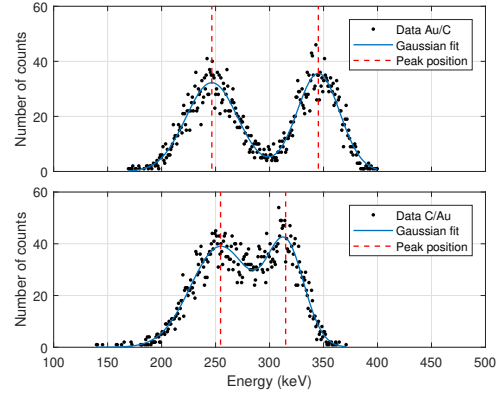


Figure 18: Thickness of target layers determined from change in energy. Upper: gold layer facing the beam. Lower: carbon layer facing the beam.

the carbon layer again on the way out.

$$\begin{aligned} E_{bf} &= E_i - t_C \left(\frac{dE}{dx} \right)_C \\ &- f_E(\theta) \left(E_i - t_C \left(\frac{dE}{dx} \right)_C \right) \\ &- \frac{t_C}{\cos(\pi - \theta)} \left(\frac{dE}{dx} \right)_C, \end{aligned}$$

where $\left(\frac{dE}{dx} \right)_C$ is the stopping power of carbon found in the table in the laboratory.

The energy change for the peak position of the distribution for gold is found as the difference between the two situations. Thus, the thickness of the carbon layer is found as

$$t_C = \frac{\Delta E_{Au}}{\left(\frac{dE}{dx} \right)_C \left(1 - f_{Au}(\theta) - \frac{1}{\cos(\theta)} \right)} \quad (9)$$

7 Nuclear reactions of protons with boron

References

- Barlow, Roger. *Statistics, A guide to the use of statistical methods in the physical sciences*. John Wiley & Sons, 1999.
- Krane, Kenneth S. *Introduction to Nuclear Physics*. 3. John Wiley & Sons, 1987.
- Paetz gen Schleck, Hans. *Nuclear Reactions: An introduction*. 3. Springer, 2014. ISBN: 978-3-642-53985-5.